Acadlore Transactions on Geosciences
https://www.acadlore.com/journals/ATG

LoRaWAN and IoT-Based Landslide Early Warning System

Muladi[1*], Sherly Yora Amarda[1], Abd Kadir Mahamad[2], Singgih Dwi Prasetyo[3,4*], Catur Harsito[5,6]

[1] Electronics Systems Engineering Technology, Faculty of Vocational Studies, State University of Malang, 65145 Malang, Indonesia
[2] Faculty of Electrical and Electronic Engineering, Universiti Tun Hussein Onn Malaysia, 86400 Batu Pahat, Johor, Malaysia
[3] Power Plant Engineering Technology, Faculty of Vocational Studies, State University of Malang, 65145 Malang, Indonesia
[4] Department of Mechanical Engineering, Faculty of Engineering, Universitas Sebelas Maret, 57126 Surakarta, Indonesia
[5] Department of Mechanical Engineering, Faculty of Vocational, Universitas Sebelas Maret, 57126 Surakarta, Indonesia
[6] Department of Mechanical Computer Industrial and Management Engineering, Kangwoon National University, 25949 Samcheok-Si, Republic of Korea

* Correspondence: Muladi (muladi@um.ac.id), Singgih Dwi Prasetyo (singgih.prasetyo.fv@um.ac.id)

Received: 05-05-2024 **Revised:** 06-07-2024 **Accepted:** 06-22-2024

Citation: Muladi, S. Y. Amarda, A. K. Mahamad, S. D. Prasetyo, and C. Harsito, "LoRaWAN and IoT-based landslide early warning system," *Acadlore Trans. Geosci.*, vol. 3, no. 2, pp. 106–122, 2024. https://doi.org/10.56578/atg030205.

Abstract: According to data from the National Disaster Management Agency (BNPB), 629 landslides occurred in 2022, resulting in 318 fatalities, 459 displaced individuals, and extensive damage to 892 buildings and public facilities. To mitigate the impacts of such events, an early warning system for landslides based on Long Range Wide Area Network (LoRaWAN) was developed, enabling more effective monitoring and response in high-risk areas. This system integrates LoRaWAN technology with a suite of sensors, including a soil moisture sensor to track moisture levels, a Global Position System (GPS) sensor to provide location data, and an accelerometer to detect tilt and acceleration changes. Sensor data were transmitted to a gateway and monitored in real time via the Blynk application. Furthermore, the relationship between Spreading Factor (SF) values, transmission distance, Time on Air (ToA), and Packet Delivery Ratio (PDR) was examined to optimize system performance. The results indicate that SF 12 provides the most reliable performance in the context of early landslide detection. Data transmission in both emergency and scheduled modes was successfully achieved, with seamless integration of the gateway and Blynk platform. This research presents a robust framework for improving disaster mitigation efforts through early detection and monitoring systems.

Keywords: Landslide early detection; Long Range Wide Area Network; Internet of Things; Spreading Factor; Time on Air; Packet Delivery Ratio

1 Introduction

Indonesia has many mountainous and hilly areas with steep slope topography. With its geographical layout being in the Interaction Zone of the Pacific and Indo-Australian Tectonic Plates [1], Indonesia has unstable soil types and complex ground movements. Apart from that, Indonesia has a tropical climate, which results in high rainfall in most parts of the country. Indonesia's natural conditions cause the country to be prone to landslides [2]. This landslide disaster is also supported by human activities which result in a decline in land quality such as agriculture, deforestation, or changes in land use like settlements [3].

Based on data from the National Disaster Management Agency (BNPB), in 2022, there were 629 landslides, causing 318 fatalities, 459 displaced, and 892 buildings and public facilities damaged. A more significant number of disasters occurred in 2020 and 2021, amounting to 2,099 and 1,321 incidents, respectively. Appropriate disaster mitigation measures for areas with the potential for landslides minimize the impacts. Effective mitigation measures

include maintaining vegetation, conducting reforestation, increasing public awareness through education, enhancing evacuation capabilities, identifying causal factors, and employing early detection systems for landslides [2].

Early detection of landslides is carried out by monitoring soil conditions and ground movement. Soil conditions and soil movement are the main parameters that determine the potential for landslides in an area. The reason is that before a landslide disaster occurs, there are changes in physical quantities in the soil. An important parameter can be seen in soil conditions, namely soil moisture. Meanwhile, monitor ground movement can be seen from the tool's slope, acceleration, and changes in location coordinates. Slope, acceleration, and changes in coordinates are essential parameters because they indicate ground movement. In addition, soil moisture is an important parameter because water stored in the soil makes it easier for the soil to fall and move. Therefore, monitoring these three parameters helps in early detection of landslides [4].

The selection of appropriate technology for early landslide detection is of paramount importance, particularly in remote areas lacking communication infrastructure, such as mountainous or forested regions. LoRaWAN technology as a wireless sensor network is the right solution. It makes it possible to transmit data in real-time because it has a wide range and is energy efficient. Therefore, it can be used in long-distance monitoring of parameters that have the potential to cause soil damage landslides [5].

In this study, an early landslide detection system was developed using LoRaWAN technology. Then the network technology was combined with soil moisture, GPS, and accelerometer sensors to measure tilt and acceleration. The monitoring application was provided to complete a reliable and user-friendly early landslide detection system that can be accessed via the internet using a desktop computer or Android device. Apart from that, this research also analyzes the effect of the SF on distance, ToA, and PDR to determine the speed and reliability of LoRaWAN performance in sending data over long distances, aiming to apply the most appropriate SF to this landslide early detection system [6]. With the LoRaWAN-based early detection system, mitigation and response to landslide-prone lands are expected to be carried out more effectively [7].

2 Related Work

2.1 Project Overview

This study aims to increase the informal settlements' resistance to landslides caused by rainfall. The Landslide Early Warning System (LEWS) was designed and implemented as a short- to medium-term risk reduction solution by the project, as long-term risk reduction solutions, like moving the endangered residents or putting in place physical mitigation measures, are currently impractical due to the significant social, political, and financial efforts needed and the potential harm they could cause to the environment. A number of social and technological obstacles need to be solved for the system to be implemented successfully. The creation of an affordable, dependable, highly resolved monitoring system in both space and time, as well as its social integration into the informal settlement in which it is deployed, provide the biggest hurdles. Only until the inhabitants for whom it is intended are on board with and trust the system will it succeed. Sufficient understanding of the population and risk perception is another essential component that dictates whether the system can have a long-lasting effect [2].

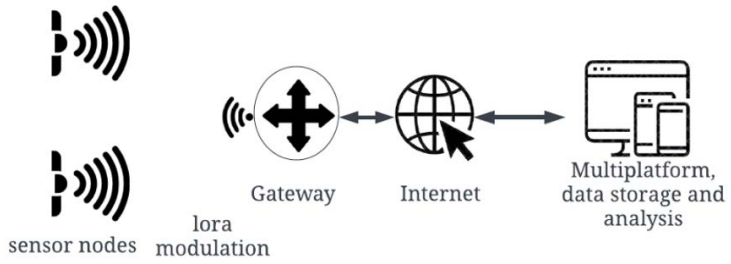

Figure 1. WSN applications using a general LoRaWAN architecture scheme

Low-power wide area networks (LPWAN) might be a useful technology to apply in Internet of Things (IoT)-oriented wireless sensor networks (WSNs). This allows the sensor nodes to function well energetically, which is essential for energy-harvesting powered devices. Overall low-cost deployment may be accomplished by utilizing newly developed LPWAN technology. Compared to high-speed telecommunications applications like big file transfers or video streaming, these structures usually require lower data rates, especially for monitoring reasons. LPWAN often requires less complicated transceiver gear. Therefore, it is frequently utilized in circumstances where little quantities of data are transferred at predefined intervals to decrease costs. The ideal point will be reached if a reasonably inexpensive solution is offered in terms of the whole system cost, as the medium access control (MAC) layer implementation frequently results in the highest expenses of the complete system. This type of performance is made possible by the Long Range (LoRa) Alliance-regulated LoRaWAN MAC layer, which is a free network

protocol that may be accessed by specialized LoRaWAN gateways. These devices are available commercially in approved outdoor variants at reasonable rates. As shown later in this study, these components may be linked together using free web services to build a dependable, fully functional, low-cost network. The network architecture was built in a star form at the MAC layer, as seen in Figure 1, with the gateway serving as the star's core. Nodes use LoRa modulation, a Semtech-developed chirp spread spectrum (CSS)-based technology, to communicate via a one-hop connection.

2.2 Potential Sources of Interference or Obstacles Impacting LoRaWAN Performance

LoRaWAN is a popular wireless communication technology for landslide monitoring, but its performance in real-world, landslide-prone areas can be affected by various factors such as dense vegetation, steep terrain, multipath interference, bad weather conditions, artificial structures, and power limitations in remote areas. Dense forests or dense vegetation can absorb and scatter radio signals, causing signal attenuation. This can be overcome by placing the antenna above the canopy, using a repeater, or choosing a frequency that is less susceptible to attenuation by foliage. Steep terrain such as mountains or cliffs hinders line-of-sight communications, which can be overcome through strategic placement of nodes on higher ground, implementation of a mesh network topology, or use of directional antennas [6].

Multipath interference caused by reflective surfaces in rocky terrain can be reduced by using antenna diversity and advanced signal processing techniques. Adverse weather conditions such as heavy rain, fog, or snow weaken the signal. Nonetheless, the use of robust modulation schemes and dynamic adjustment of communication parameters based on environmental monitoring can enhance signal resilience under such conditions. Artificial structures block or reflect signals. Therefore, the implementation of a thorough site survey and the design of a network with redundancy help avoid communication disruptions [6].

2.3 Advantages of this Study

Although many existing landslide monitoring systems are effective, they are often expensive and require complex infrastructure, limiting their use in remote areas or areas with limited resources. This research is an alternative solution that is more affordable and easier to mobilize. A reliable real-time monitoring system is needed that can operate in remote, difficult, and landslide-prone areas. The proposed system aims to fill this gap by leveraging the long-range and low-power communication capabilities of LoRaWAN [7].

This study aims to enable LoRaWAN technology to be implemented in existing early warning systems to increase their effectiveness, especially in terms of timely data transmission and warning generation and minimize false alarms and missed detections. Current systems sometimes struggle to balance sensitivity and specificity, resulting in false alarms or missed detections.

3 Methodology

3.1 Block Diagram System

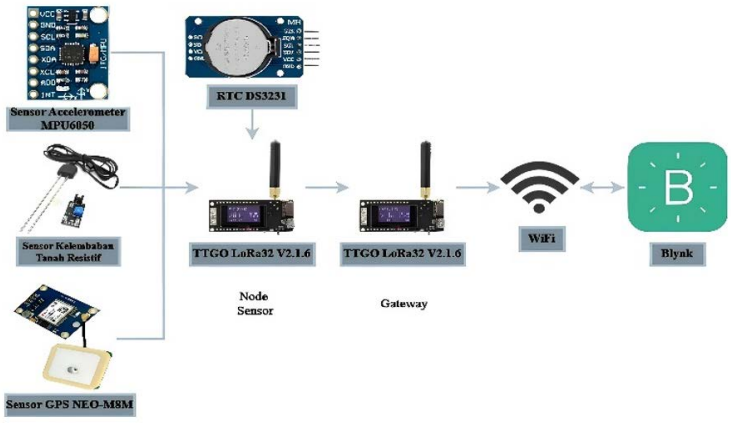

Figure 2. Block diagram system

This circuit below illustrates how TTGO LoRa32 V2.1.6 is connected to several sensors. The soil moisture sensor is connected to the LoRa module via the analog pin, namely GPIO36; the NEO M8M GPS sensor is connected to the LoRa module via the RX pin, which is connected to GPIO4, and the TX pin, which is connected to GPIO25. RTC DS3231 is connected to the LoRa module via the SDA pin, which is connected to GPIO21, and the SCL pin, which is connected to GPIO22. Likewise, the MPU6050 is connected to the LoRa module via the SDA pin, which

is connected to GPIO21, the SCL pin, which is connected to GPIO22, and the AD0 pin, which is connected to 3.3V. The system block diagram is shown in Figure 2.

3.2 Flowchart System

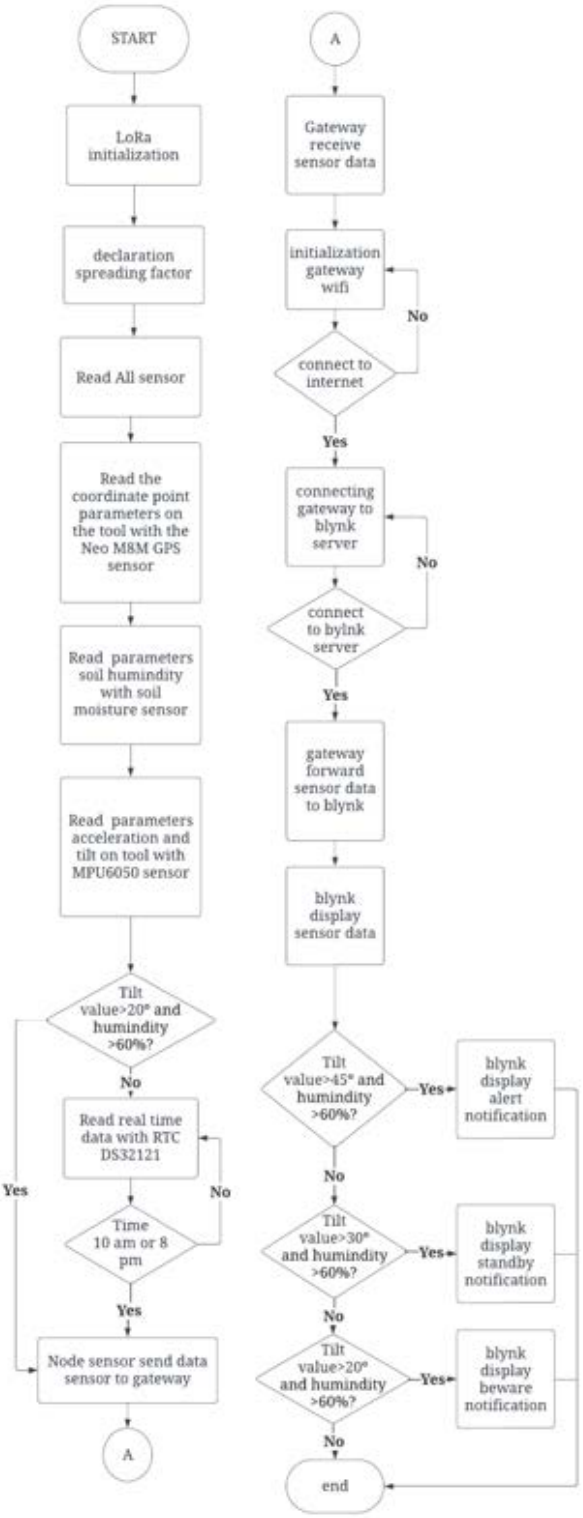

Figure 3. Flowchart system

The work process flow in Figure 3 explains the working system of this tool. This tool has two modes, namely, scheduling and emergency modes. The sensor node sends sensor data to the gateway in real-time according to the scheduling set by the user. The sensor node also sends sensor data to the gateway in the emergency mode if the slope

value exceeds the standard limit ($> 20°$) and the soil moisture value ($> 60°\%$). Then the gateway that has received data from the sensor node forwards it to Blynk for display. If the slope data displayed includes alert, standby, or warning conditions, then Blynk will warn of landslides according to the category. The alert condition represents the initial stage of landslide risk and is defined when the slope is between $20°$ and $30°$ with a moisture level exceeding 60%. The standby condition, indicating an elevated risk of landslides, is triggered when the slope is between $30°$ and $45°$ and the moisture level remains above 60%. A warning condition signals an imminent landslide, with slope values exceeding $45°$ and moisture levels surpassing 60% [8]. When checking data, the limit or threshold number was set to absolute, which means that positive and negative numbers are considered the same [9].

3.3 System Details

3.3.1 Schematics of the electrical system

This circuit below illustrates how TTGO LoRa32 V2.1.6 is connected to several sensors. The soil moisture sensor is connected to the LoRa module via the analog pin, namely GPIO36; the NEO M8M GPS sensor is connected to the LoRa module via the RX pin, which is connected to GPIO4, and the TX pin, which is connected to GPIO25. RTC DS3231 is connected to the LoRa module via the SDA pin, which is connected to GPIO21, and the SCL pin, which is connected to GPIO22 [10, 11]. Likewise, the MPU6050 is connected to the LoRa module via the SDA pin, which is connected to GPIO21, the SCL pin to GPIO22, and the AD 0 pin to 3.3 V , which is connected to each device. Figure 4 shows the details. Table 1 shows the overall prices that are much cheaper than the products marketed on the website, which can be seen in Table 2, where the things offered are the same, namely reliability and features. Moreover, there are additional application features where users can monitor easier anytime and anywhere using Blynk.

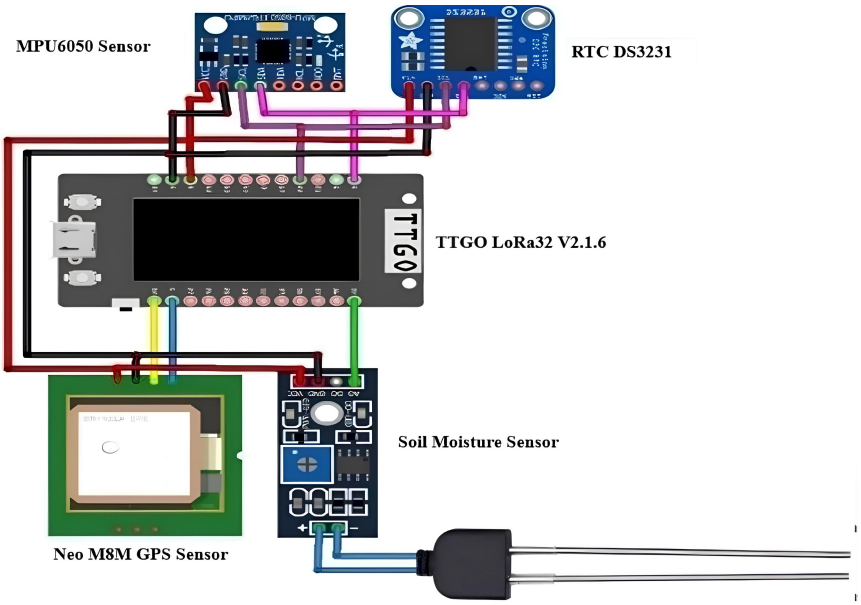

Figure 4. Schematics of the electrical system

Table 1. Component prices

Component	Amount	Price
Sensor Mpp 6050	1	Rp 255.000
RTC DS3231	1	Rp 50.000
TTGO LoRA ESP32 V2.1.6	2	Rp 1.000.000
Sensor GPS NEO M8M	1	Rp 250.000
Sensor soil moisture V2	1	Rp 25.000
Battery 18650	4	Rp 150.000
Box	1	Rp 100.000
Total	Rp 1.830.000	

Table 2. Comparison of similar tools

No.	Price	Description	Usage/Application	Buying Link
1	Rp 45.200.000	LEWS	A tool used to detect landslides using GSM/SMS network; EWS early warning system for landslides via GSM early warning radio;	https://www.tokopedia.com/rekomendasi/1319623625?utm
2	Rp 97.500.000	Landslide disaster early warning system	A tool used to detect landslides; Using GSM/SMS network; Using a radio network for backup if there is no GSM signal; Radio signal distance up to 5 km;	https://www.tokopedia.com/discovery/rekomendasi?recomProdId==1345791746 & utm
3	Rp 300.000.000	EWS application + landslide + fire + flood sensor tool	EWS App + fire + flood + landslide sensor tool has features; Landslide monitoring and video (CCTV) via Web and mobile applications, recording video of events.	https://ekosis.id/d/fns-lidi-sawit-9243/aplikasi-ews-alat-sensor-longsor-tanah-kebakaran-banjir-5427?srsltid=AfmBOookYStx xwn6c3WGxW8Nk0g3rOM9Y-Omik3fNVzdfDOnqJO6Q-3Lo

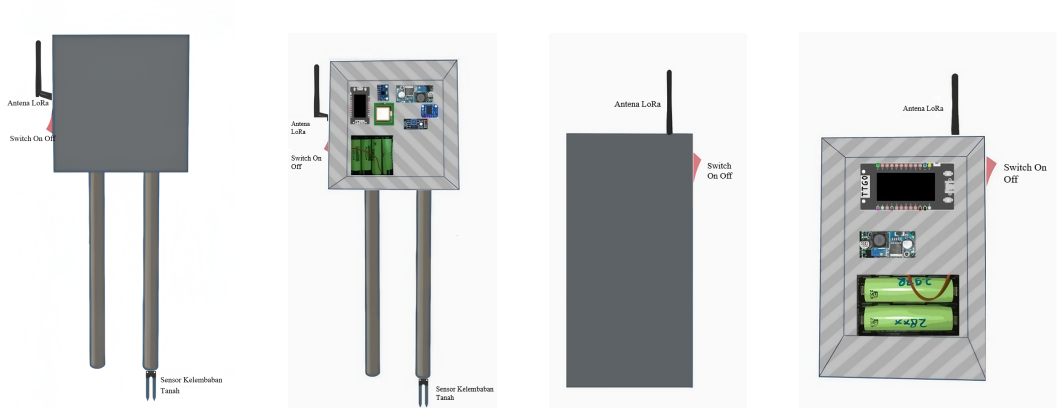

(a) (b) (c) (d)

Figure 5. Multiplatform design (a) External view of the sensor node tool designed; (b) Internal view of the sensor node tool designed; (c) External view of the gateway tool; (d) Internal view of the gateway tool designed

3.3.2 Mechanical design

The sensor node is equipped with a cube-shaped casing, measuring 20 cm × 20 cm × 13 cm (length × width × height). In addition, the sensor node is equipped with a tubular pipe with a length of 1 m and a diameter of 2 cm. Meanwhile, the gateway has a block-shaped casing, measuring 14.5 cm × 9 cm ×5 cm (length × width × height). The mechanical design components can be seen in Figure 5.

3.3.3 Design application

The Blynk application was designed by adjusting the type of input available on each widget using programming. The application displays the results of measured values for several parameters such as soil moisture values, X acceleration, Y acceleration, Z acceleration, slope, latitude, and longitude. In addition, the Blynk application was designed to display notifications through programming settings. When the sensor readings fall within the initial alert category, the Blynk application triggers a notification indicating alert, signifying the initial potential for a landslide [12–14]. As the sensor data escalates to a higher-risk alert category, a standby notification is triggered, reinforcing the increased likelihood of a landslide event. Finally, when the system identifies the conditions that match the warning category, the application displays a caution notification, indicating that a landslide has occurred [15–18]. The application design is shown in Figure 6.

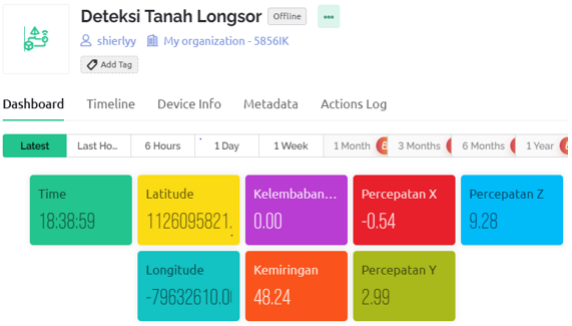

(a)

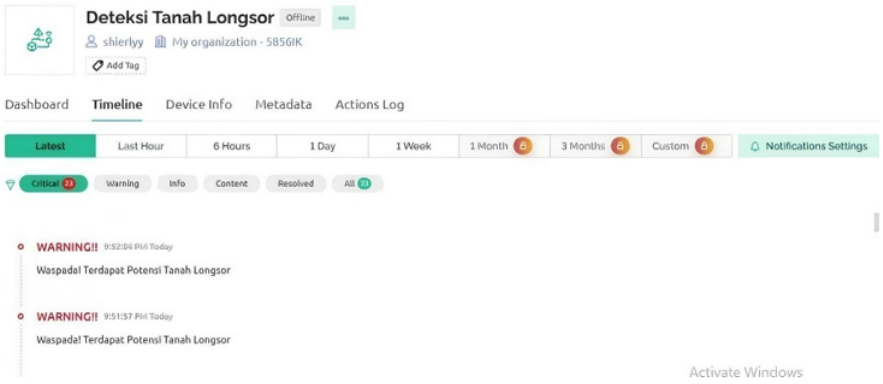

(b)

(c)

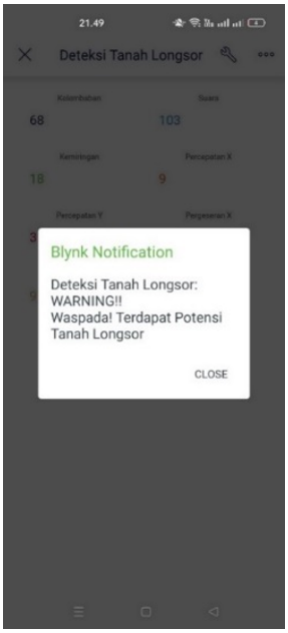

(d)

Figure 6. Multiplatform design (a) Main page website; (b) Notification page website; (c) Main page application; (d) Notification page application

3.4 Calibration Method

3.4.1 Calibration of the soil moisture sensor

With the wet and dry weights now known, the gravimetric soil water content can be calculated as follows:

$$\text{Water Content} = (\text{Wet Weight} - \text{Dry Weight})/(\text{Dry Weight} * 100) \quad (1)$$

Soil density is needed to convert soil water content gravimetrically into volumetric air content. The density of this sample can be measured using the Soil Core Sampler SEC 0200, for example. Density is the weight of soil based on its area.

$$\text{VWC} = (\text{ Gravimetric Soil Air }) \times (\text{ Bulk Density }) \tag{2}$$

An important thing to consider is establishing offsets or calibration curves as required for the IoT installation [19–23].

3.4.2 Calibration of the sensor GPS M8M

For the electrical specifications from the datasheet, the limit values given are in accordance with the Absolute Maximum Rating System (IEC 134), as shown in Figure 6. Stress of the above one or more limit values may cause permanent damage to the device. This is a stressful course rating, and operation of the device under these or other conditions above those given in the characteristics section of the specification is not implied. Exposure to these limitations for an extended period may affect device reliability [24–26].

Parameter	Symbol	Module	Condition	Min	Max	Units
Power supply voltage	VCC	All		-0.5	3.6	V
Backup battery voltage	V_BCKP	All		-0.5	3.6	V
USB supply voltage	VDD_USB	All		-0.5	3.6	V
Input pin voltage	Vin	All		-0.5	3.6	V
	Vin_usb	All		-0.5	VDD_USB	V
DC current trough any digital I/O pin (except supplies)	Ipin				10	mA
VCC_RF output current	ICC_RF	All			100	mA
Input power at RF_IN	Prfin	All	source impedance = 50 Ω, continuous wave		15	dBm
Storage temperature	Tstg	NEO-M8M NEO-M8N/M8Q		-40 -40	105 85	°C °C

Figure 7. Electrical specifications of the NEO M8M

The GPS module generally consists of a GPS device composed of three segments: satellite, monitoring and receiver. A GPS receiver must lock on to the signals of at least three satellites to calculate 2D position (latitude and longitude) and track movement. If the GPS receiver can receive four or more satellites, the GPS can display 3D position (latitude, longitude and altitude). GPS NEO M8M is a GPS module that receives four satellites to collect latitude, longitude, and altitude data. Figure 7 shows the display of the measurement results of the GPS NEO M8M module, which captures data in the form of position data captured in the GPS module [27–29].

3.4.3 Calibration of the sensor accelerometer MPU6050

The accelerometer was utilized to detect gravity to obtain a point of comparison. The accelerometer is noisy. Therefore, any acceleration other than rotation might skew the readings. Nevertheless, basic trigonometry can be used to transform these raw acceleration numbers to pitch and roll angles with respect to the horizontal. A supplementary filter can be used to merge the accelerometer pitch and roll angles and integrated gyroscope. Measuring just 0.1% of the accelerometer, the complementary filter adds around 99.9% of the gyroscope angle readings. Stable angle measurements connected to the horizontal reference are produced by the complementary filter, which magically calculates this each time around the Arduino's loop function. These angles also correct for the gyroscope's drift and are acceleration invariant [30–33].

The mean average of a few hundred raw gyro readings at startup was subtracted from the raw values obtained throughout operation to calibrate the gyroscope. After placing the accelerometer on flat ground, the average raw value was calculated, and that number was deducted from the raw data and calibrated by the accelerometer. To avoid calibration every time when starting up the accelerometer, it is also feasible to keep its values in Electrically Erasable Programmable Read-Only Memory (EEPROM) [34, 35].

4 Results

4.1 LoRaWAN Performance Testing at 100 m

LoRaWAN testing was carried out at 100 m by comparing the effect of SFs 10, 11, and 12 on ToA and PDR during the day and night. To determine the effect of SF, the data was sent 30 times to look for the ToA value for each piece of data. Then, based on the data, the overall average ToA and PDR results of all the data sent were obtained. The 100 m LoRaWAN distance test results are shown in Table 3 and Table 4.

Table 3. LoRaWAN test distance of 100 m during the day

SF	Min ToA	Max ToA	Rata-rata ToA	PDR
7	2.428	2.503	2.463	100%
8	2.436	2.497	2.469	100%
9	2.428	2.5	2.465	100%
10	2.356	2.5	2.47	100%
11	2.432	2.51	2.476	100%
12	2.468	4.353	3.225	100%

Table 4. LoRaWAN test distance of 100 m at night

SF	Min ToA	Max ToA	Average ToA	PDR
7	0.142	0.201	0.167	100%
8	0.145	0.202	0.17	100%
9	0.148	0.202	0.176	100%
10	0.152	0.204	0.181	100%
11	0.16	0.217	0.195	100%
12	0.177	0.229	0.209	100%

4.2 LoRaWAN Performance Testing at 300 m

LoRaWAN testing was carried out in the same way at 300 m. Data was sent 30 times, and ToA was obtained from each piece of data. Then, based on this data, the overall average ToA and PDR results of all the data sent were obtained. The 300 m LoRaWAN distance test results are shown in Table 5 and Table 6.

Table 5. LoRaWAN test distance of 300 m during the day

SF	Min ToA	Max ToA	Average ToA	PDR
7	2.432	2.467	2.449	6%
8	2.465	2.563	2.514	6%
9	2.455	2.643	2.53	13%
10	2.431	2.647	2.545	20%
11	2.416	2.641	2.55	56%
12	2.417	2.654	2.559	83%

Table 6. LoRaWAN test distance of 300 m at night

SF	Min ToA	Max ToA	Average ToA	PDR
7	0.148	0.217	0.149	10%
8	0.127	0.214	0.172	16%
9	0.146	0.184	0.163	16%
10	0.145	0.207	0.174	26%
11	0.116	0.116	0.182	56%
12	0.153	0.221	0.19	93%

From the two tables above, it is known that data sending at night produces a shorter ToA and a greater PDR than that during the day. Therefore, based on this data, data transmission at night is more reliable than that during the day because there are many obstacles or noises during the day. The table above shows that the greater the SF, the greater the percentage of data sent. However, the resulting ToA takes longer. Apart from that, when compared with data sending at 100 m, the farther the range, the smaller the PDR value and the longer the ToA. However, the ToA resulting from a higher SF and a more extended range has a value close to the ToA with a small SF and a closer range. Therefore, based on the data above, it was found that it is better to use SF 12 because, it can produce a high PDR at 300 m.

4.3 LoRaWAN Performance Testing at 500 m

LoRaWAN testing was carried out in the same way at 500 m. Data was sent 30 times, and ToA was obtained from each of the 30 pieces of data. Then, based on this data, the overall average ToA and PDR results of all the data

sent were obtained. The 500 m LoRaWAN distance test results are shown in Table 7 and Table 8.

Table 7. LoRaWAN test distance of 500 m during the day

SF	Min ToA	Max ToA	Average ToA	PDR
7	2.414	2.414	2.414	3%
8	2.446	2.446	2.446	3%
9	2.438	2.467	2.452	6%
10	2.534	2.568	2.549	10%
11	2.591	2.657	2.625	16%
12	2.543	2.687	2.648	26%

Table 8. LoRaWAN test distance of 500 m at night

SF	Min ToA	Max ToA	Rata-rata ToA	PDR
7	0.175	0.175	0.175	3%
8	0.189	0.189	0.189	3%
9	0.201	0.201	0.201	3%
10	0.205	0.205	0.205	3%
11	0.223	3.426	2.23	16%
12	0.232	3.744	160.595	30%

From the two tables above, it is known that data sending at night produces a shorter ToA and a greater PDR than that during the day. Therefore, based on this data, data transmission at night is more reliable than that during the day because there are many obstacles or noises during the day. The table above shows that the greater the SF, the greater the percentage of data sent. However, the resulting ToA takes longer. Apart from that, when compared with data sending at 100 m and 300 m, the longer the range, the smaller the PDR value and the ToA. However, the ToA resulting from a higher SF and a farther range has a value close to the ToA with a small SF and a closer range. Therefore, based on the data above, it was found that it is better to use SF 12 at 500 m because it is still able to receive data even though there is still a lot of packet loss. Therefore, reliability in sending data at 500 m has poor results unless the antenna with a larger dB can be increased.

4.4 Testing of Soil Moisture Sensor

Soil moisture sensor testing was carried out to determine the sensor accuracy level by comparing the capacitive soil moisture readings values with a soil moisture meter. Where it can be seen from the table above that the average error value of the soil moisture meter reading and the sensor value is 0.88%, which is smaller than the sensor accuracy limit of ±2%. From these results, it can be concluded that the soil moisture sensor has an accuracy level of 99.12% and can read changes in soil moisture well. The results of the soil moisture sensor test are shown in Table 9.

Table 9. Soil moisture sensor testing

No.	Average Soil Moisture Sensor(%)	Average Soil Moisture Meter(%)	Error (%)
1	0	0	0,0
2	20,26	20	1,3
3	40,14	40	0,35
4	41,03	40	2,58
5	50,05	50	0,1
6	60,21	60	0,35
7	61,12	60	1,87
8	71,02	70	1,46
9	80,34	80	0,43
10	90,28	90	0,31
	Average error (%)	0,88	

4.5 Testing of the Sensor GPS NEO M8M

The NEO M8M GPS sensor was tested to determine the sensor accuracy level by comparing the sensor readings' coordinate values with Google Maps. The comparison values of the coordinate points detected by the NEO M8M

GPS sensor with Google Maps are the same. From these results, it can be concluded that the NEO M8M GPS sensor used is accurate. The results of the GPS sensor test are shown in Table 10.

Table 10. Testing of the GPS sensor

No.	Latitude Sensor	Longitude Sensor	Latitude Google Maps	Longitude Google Maps
1	-7.960720	112.614832	-7.960720	112.614832
2	-7.963314	112.609523	-7.963314	112.609523
3	-7.963345	112.609605	-7.963345	112.609605
4	-7.877753	112.522800	-7.877753	112.522800
5	-7.962518	112.618246	-7.962518	112.618246
6	-7.961554	112.616980	-7.961554	112.616980
7	-7.959982	112.620724	-7.959982	112.620724
8	-7.961738	112.617304	-7.961738	112.617304
9	-7.962338	112.616935	-7.962338	112.616935
10	-7.960127	112.620946	-7.960127	112.620946

4.6 Sensor Accelerometer MPU6050

Table 11. Accelerometer MPU6050

No.	Condition	Average Sensor Tilt (°)	Average Arc Slope (°)	Error (%)
1	No movement	0,25	0	0,00
2	No movement	0,30	0	0,00
3	No movement	0,69	0	0,00
4	No movement	0,50	0	0,00
5	There is movement.	30,14	30	0,47
6	There is movement.	41,77	40	4,43
7	There is movement.	54,15	54	0,28
8	There is movement.	20,19	20	0,95
9	There is movement.	45,84	45	1,87
10	There is movement.	0,15	62	1,11
Average error (%)				0,82

Testing of the MPU6050 accelerometer sensor was carried out so that it could measure tilt and acceleration values. The accuracy level of the MPU6050 sensor was determined by comparing the tilt value with an arc-measuring instrument and adjusting the acceleration values for the X, Y, and Z axes. The results of the accelerometer MPU6050 sensor test are shown in Table 11.

From the table above, the average error is 0.82%, smaller than the sensor accuracy limit of ±2%. From these results, it can be concluded that the MPU6050 sensor has an accuracy level of 99.18% and can read slope values well. The slope data was taken by moving the tool according to the roll axis (slope to the x-axis) and pitch (slope to the y-axis). The acceleration data values of the X, Y, and Z axes are shown in the table above. In a stationary position, the X and Y axes produced an acceleration value of 0 or close to 0, and the Z axis corresponded to the earth's gravity value, namely 9.8. Meanwhile, when there was movement, it produced an acceleration of more than 1 m/s^2. From these results, it can be concluded that the MPU6050 sensor can read the acceleration values. When the tool is stationary, the acceleration value returns to 0 or near 0. The acceleration parameter results of the accelerometer sensor testing are shown in Table 12.

4.7 Overall Testing of the Scheduling Mode at 10 am

Testing of the entire system at 10 am for 5 minutes was carried out to determine the accuracy of data sending according to the schedule that had been arranged. The data collection process was carried out on dry and moist soil with the equipment in a stationary condition. Table 13 shows the successful data sending from the sensor node to the gateway and from the gateway to Blynk so that Blynk can display appropriate and accurate sensor data. The conditions are safe because the tool has no movement, and the resulting sensor data does not exceed the predetermined safe limits.

Table 12. Accelerometer MPU6050

No.	Condition	Average X Axis Acceleration $(\mathbf{m/s^2})$	Average Y Axis Acceleration $(\mathbf{m/s^2})$	Average Z Axis Acceleration $(\mathbf{m/s^2})$
1	No movement	0,05	0,06	9,8
2	No movement	0,30	0,06	9,8
3	No movement	0,37	0,30	9,8
4	No movement	0,52	0,43	9,8
5	No movement	0,22	0,14	9,8
6	There is movement.	0,28	2,45	10,5
7	There is movement.	7,23	0,71	5,99
8	There is movement.	0,14	4,34	9,2
9	There is movement.	0,15	6,21	8,3
10	There is movement.	8,23	0,15	6,51

Table 13. Entire testing of the scheduling mode at 10 am

No.	Condition	Humidity	Tilt	Acceleration x	Acceleration y	Acceleration z	Latitude	Longitude	Result
1	Silent	0	0,16	0,5	9,28	0,15	-7.963261	112.609821	Safe
2	Silent	0	0,36	0,38	9,28	0,46	-7.963261	112.609821	Safe
3	Silent	13	1,23	0,26	9,8	0,58	-7.963261	112.609821	Safe
4	Silent	18	2,42	0,04	9,6	0,72	-7.963261	112.609821	Safe
5	Silent	24	0,59	0,28	9,6	0,54	-7.963261	112.609821	Safe
6	Silent	25	1,96	0,46	9,8	0,76	-7.963261	112.609821	Safe
7	Silent	30	3,71	0,58	9,8	0,23	-7.963261	112.609821	Safe
8	Silent	32	2,38	0,87	9,7	0,31	-7.963261	112.609821	Safe
9	Silent	34	1,45	0,79	9,7	0,43	-7.963261	112.609821	Safe
10	Silent	35	0,31	0,45	9,6	0,54	-7.963261	112.609821	Safe

4.8 Overall Testing of the Scheduling Mode at 8 pm

Testing of the entire system at 8 pm for 5 minutes was carried out to determine the accuracy of data sending according to the schedule that had been arranged. The data collection process was carried out on dry and moist soil with the equipment in a stationary condition. Table 14 shows the successful data sending from the sensor node to the gateway and from the gateway to Blynk so that Blynk can display appropriate and accurate sensor data.

4.9 Overall Testing of the Emergency Mode

This test was carried out to determine whether the sensor node can send data in the emergency mode when the sensor condition exceeds the normal limits. Data was collected on wet ground with the tool moving concerning roll and pitch angles. Table 15 shows that the sensor node successfully sent data to the gateway when the tilt sensor was more than 20° and the soil moisture sensor was more than 60%. Then, the gateway successfully forwarded the data to Blynk so that Blynk could display accurate sensor data and notifications by the threshold that had been set. An alert notification will be displayed when the slope value is between 20° and 30° with a moisture level exceeding 60%. A standby notification will be displayed when the slope is between 30° and 45° and the moisture level remains above 60%. A warning notification will be displayed when the slope is in the range of more than 45° and the humidity value is more than 60%.

4.10 Display Results and Notifications Using Blynk

The tables above display the Blynk application and website in the scheduling mode test, carried out at 10 am and 8 pm. Blynk can display the sensor data at the scheduled time. The tables show the Blynk application and website display, along with notifications in the emergency mode testing. Blynk can display data when the sensor value exceeds the safe limit. Apart from that, Blynk can also display alerts, standby, or warning notifications according to the sensor values displayed. Blynk display results and notifications are shown in Figure 8 and Figure 9.

Table 14. Entire testing of the scheduling mode at 8 pm

No.	Condition	Humidity	Tilt	Acceleration x	Acceleration y	Acceleration z	Latitude	Longitude	Result
1	Silent	0	0,14	0,05	9,28	0,06	-7.963261	112.609821	Safe
2	Silent	0	0,35	0,34	9,28	0,03	-7.963261	112.609821	Safe
3	Silent	27	0,26	0,25	9,6	0,13	-7.963261	112.609821	Safe
4	Silent	30	2,53	0,07	9,7	37	-7.963261	112.609821	Safe
5	Silent	33	0,12	0,06	9,6	0,21	-7.963261	112.609821	Safe
6	Silent	37	1,45	0,15	9,8	0,35	-7.963261	112.609821	Safe
7	Silent	40	2,67	0,24	9,8	0,45	-7.963261	112.609821	Safe
8	Silent	39	2,41	0,36	9,6	0,86	-7.963261	112.609821	Safe
9	Silent	42	0,45	0,06	9,7	0,34	-7.963261	112.609821	Safe
10	Silent	45	3,31	0,14	9,6	0,23	-7.963261	112.609821	Safe

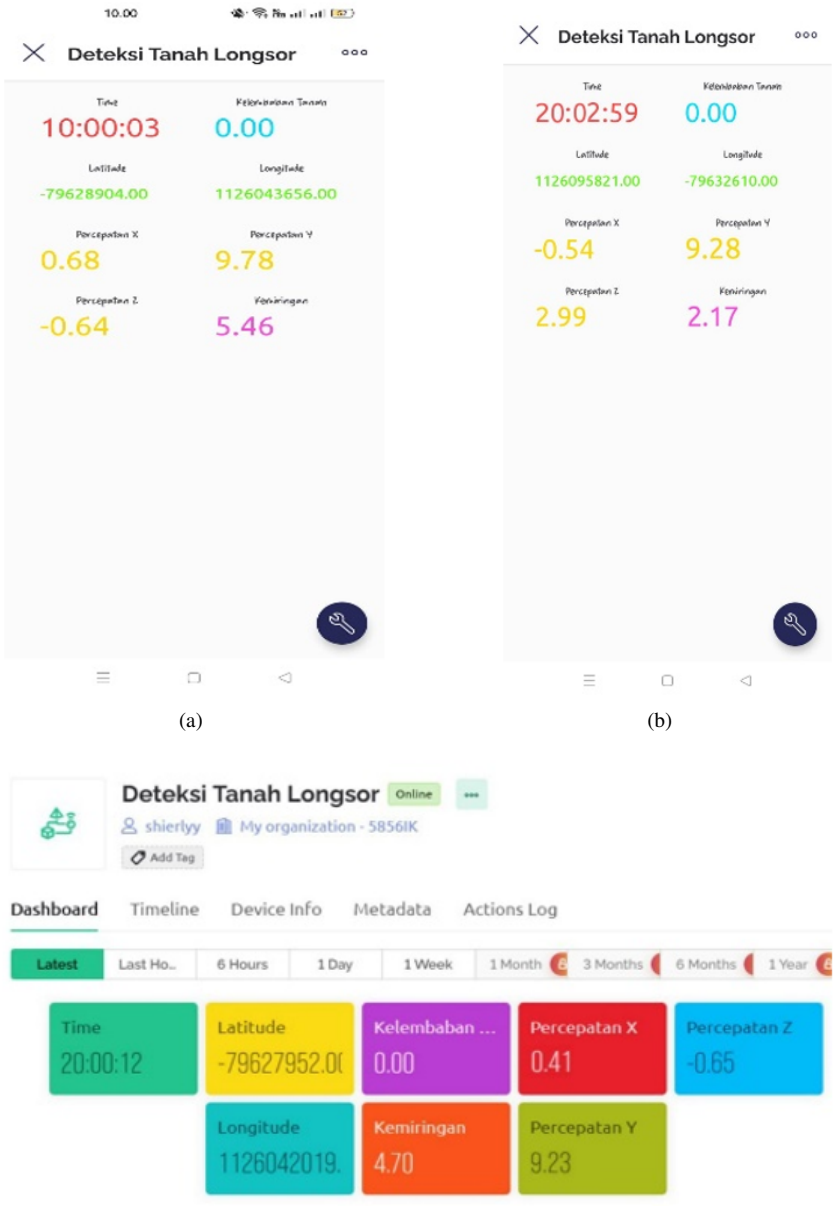

(a) (b)

(c)

Figure 8. Application testing according to the schedule (a) Testing application of the home page at 10 am; (b) Testing application of the home page at 8 pm; (c) Home page of the scheduling mode testing website

Table 15. Entire testing of the emergency mode

No.	Condition	Humidity	Tilt	Acceleration x	Acceleration y	Acceleration z	Latitude	Longitude	Result
1	There is movement.	60	22,6	2,56	8,9	0,16	-7.963261	112.609821	alert
2	There is movement.	62	22,8	3,86	8,7	0,24	-7.963261	112.609821	alert
3	There is movement.	65	35,6	4,96	7,6	0,35	-7.963261	112.609821	standby
4	There is movement.	69	39,6	5,65	6,7	0,03	-7.963261	112.609821	standby
5	There is movement.	72	43,5	0,23	6,0	6,23	-7.963261	112.609821	standby
6	There is movement.	76	53,6	0,75	5,7	6,75	-7.963261	112.609821	beware
7	There is movement.	82	59,7	0,48	4,2	6,48	-7.963261	112.609821	beware
8	There is movement.	85	64,5	0,34	3,4	7,34	-7.963261	112.609821	beware
9	There is movement.	94	68,3	0,19	2,8	8,19	-7.963261	112.609821	beware
10	There is movement.	96	75,6	0,57	2,5	8,57	-7.963261	112.609821	beware

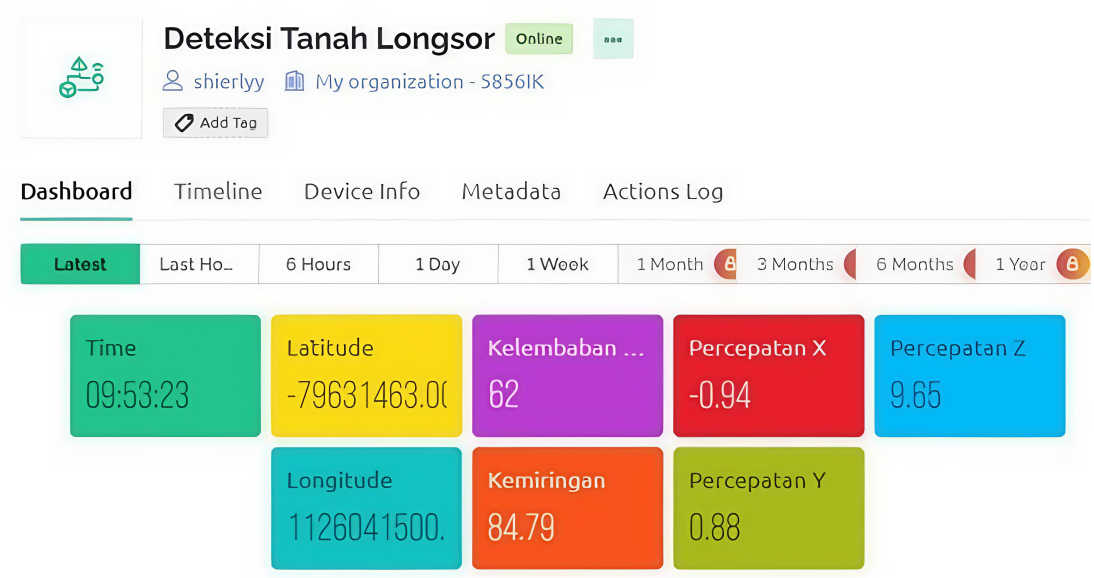

(a)

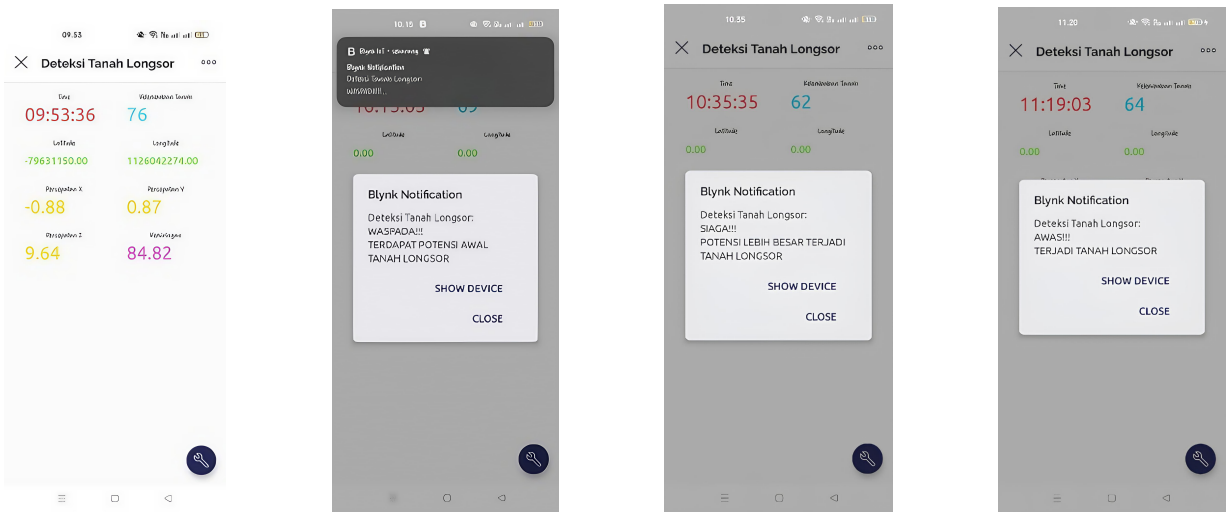

(b) (c) (d) (e)

Figure 9. Testing of the multiplatform emergency mode (a) Home page of the emergency mode testing website; (b) Home page of the emergency mode testing application; (c) Alert notification; (d) Alert notification level; (e) Alert notification level

5 Discussion

5.1 Research for Future Work

The LoRaWAN system can collect real-time data from sensors installed in various locations that are prone to landslides. This data includes information such as soil moisture, ground movement, and vibrations, which indicate the potential for landslides. When the data on soil moisture, latitude, longitude, and acceleration continues to increase until it reaches a critical threshold, this can be immediately sent to the monitoring center. Thus, local authorities can use this data to dynamically update risk assessments and provide early warnings to local communities.

Data collected from LoRaWAN systems can be integrated into the Geographic Information System (GIS) already used by local authorities. This enables the visualization of data in interactive risk maps, which can be used for further spatial analysis and monitoring of conditions in the field. Data from sensors can be mapped in real-time using topographic maps of the area. Areas with significant changes in conditions can be flagged and further analyzed, allowing emergency response teams to prioritize high-risk areas.

6 Conclusions

The data transmission scheme in the landslide early detection system consists of sensor nodes, gateways, and monitoring applications. At the sensor node, there are several sensor modules such as the soil moisture sensor, MPU6050 sensor, NEO M8M GPS sensor, RTC DS3231, and the TTGO LoRa32 V2.1.6 module as a data processor and sender to the gateway. The gateway also has the same LoRa module, which forwards data to the Blynk application using a WiFi connection. Then, the data can be displayed in the Blynk application. In LoRaWAN performance testing, it was found that SF 12 is the best SF to be implemented in this landslide early detection tool because it can send data to a more extended range, namely 300 m, with high PDR and ToA values comparable to lower SFs at shorter ranges. After testing the entire system, the testing results were obtained, indicating that the system can run according to plan. Data was sent successfully by the sensor node to the gateway in the emergency or scheduling mode. The gateway also successfully forwarded data to Blynk so that Blynk could display the sensor data and notifications corresponding to the data's conditions.

Data Availability

The data used to support the findings of this study are available from the corresponding author upon request.

Acknowledgments

This work is supported by the Internal Research Grant 2024 from Universitas Negeri Malang under contract number 4.4.301/UN32.14.1/LT/2024.

Conflicts of Interest

The authors declare that they have no conflicts of interest.

References

[1] A. Taqwa, M. Fadhli, S. Soim, A. S. Handayani, and Suroso, "Prototype design of landslide early detection system using LoRa and IoT," in *4th Forum in Research, Science, and Technology (FIRST-T1-T2-2020)*, 2021, pp. 495–499. https://doi.org/10.2991/ahe.k.210205.084

[2] M. Gamperl, J. Singer, and K. Thuro, "Internet of Things geosensor network for cost-effective landslide early warning systems," *Sensors*, vol. 21, no. 8, pp. 1–23, 2021. https://doi.org/10.3390/s21082609

[3] N. P. Anisa, N. F. B. A. Rahman, and S. Saehana, "Prototype of landslide detection alarm based on IoT (Internet of Things) as a physics learning medium," *J. Environ. Sustain. Educ.*, vol. 2, no. 1, pp. 1–5, 2024. https://doi.org/10.62672/joease.v2i1.26

[4] J. D. Prasetya, A. H. Pratomo, and S. P. Tahalea, "Lorawan technologies to enable landslide disaster prone areas monitoring," in *Proceeding of LPPM UPN "Veteran" Yogyakarta Conference Series 2020–Engineering and Science Series*, 2020, pp. 376–384. https://doi.org/10.31098/ESS.V1I1.131

[5] A. B. A. Mohlisin and S. F. S. Adnan, "Palm, rubber plantation and paddy field soil monitoring system using LoRa," in *2022 IEEE Industrial Electronics and Applications Conference (IEACon), Kuala Lumpur, Malaysia,*, vol. 2022, 2022, pp. 223–228. https://doi.org/10.1109/ieacon55029.2022.9951833

[6] M. Alipio and M. Bures, "Current testing and performance evaluation methodologies of LoRa and LoRaWAN in IoT applications: Classification, issues, and future directives," *Inter. Things*, vol. 25, p. 101053, 2024. https://doi.org/10.1016/j.iot.2023.101053

[7] M. Esposito, L. Palma, A. Belli, L. Sabbatini, and P. Pierleoni, "Recent advances in Internet of Things solutions for early warning systems: A review," *Sensors*, vol. 22, no. 6, p. 2124, 2022. https://doi.org/10.3390/s22062124

[8] S. Bagwari, A. Gehlot, R. Singh, N. Priyadarshi, and B. Khan, "Low-cost sensor-based and LoRaWAN opportunities for landslide monitoring systems on IoT platform: A review," *IEEE Access*, vol. 10, pp. 7107–7127, 2022. https://doi.org/10.1109/access.2021.3137841

[9] A. Inbavalli, R. Praveena, and M. Kaviya, "Assessing metrics using LoRa technology for real-time landslide monitoring within an IoT framework," in *2024 4th International Conference on Pervasive Computing and Social Networking (ICPCSN), Salem, India*, vol. 2024, 2024, pp. 656–662. https://doi.org/10.1109/icpcsn62568.2024.00109

[10] P. Sérgio Francisco, N. J. Gomes, and J. C. Batchelor, "Two solutions of soil moisture sensing with RFID for landslide monitoring," *Sensors*, vol. 18, no. 2, p. 452, 2018. https://doi.org/10.3390/s18020452

[11] M. Ragnoli, A. Leoni, G. Barile, G. Ferri, and V. Stornelli, "LoRa-based wireless sensors network for rockfall and landslide monitoring: A case study in Pantelleria Island with portable LoRaWAN access," *J. Low Power Electron. Appl.*, vol. 12, no. 3, p. 47, 2022. https://doi.org/10.3390/jlpea12030047

[12] N. F. Rachman, Sunardi, A. Aghastya, W. A. Wirawan, and N. D. O. Putri, "Simulation of early warning system in landslides and flooding with IoT," in *AIP Conference Proceedings*, 2023. https://doi.org/10.1063/5.0114918

[13] N. Sidek, M. A. Hafez, A. Idris, M. F. Arshad, and M. H. Pauzi, "Landslide-based early warning using Wi-Fi and LoRa technology," *Math. Stat. Eng. Appl.*, vol. 71, no. 4, pp. 7209–7225, 2022. https://doi.org/10.17762/msea.v71i4.1339

[14] U. Patel, A. Yadav, and K. Yadav, "IOT based landslide detection," 2022. https://easychair.org/publications/preprint/Kr6l

[15] A. Reethika, T. M. Prakash, S. K. Pranao, D. K. Raj, and K. R. Kumar, "Automatic sensor network analysis for landslide detection system," *J. Phys.: Conf. Ser.*, vol. 1916, p. 012120, 1916. https://doi.org/https://doi.org/10.1088/1742-6596/1916/1/012120

[16] S. K. Mittapally and R. K. Marichamy, "Wireless sensor networks and real-time slope monitoring: A brief review," in *Second International Conference on Emerging Trends in Engineering (ICETE 2023)*, 2023, pp. 1307–1317. https://doi.org/10.2991/978-94-6463-252-1_131

[17] S. Balamurugan, G. Sasi, A. Mohanapriya, D. FaridhaBanu, S. Ramalingam, and B. SakthiKumar, "An IoT based natural disaster monitoring for railway accident warning alert system," in *2022 3rd International Conference on Communication, Computing and Industry 4.0 (C2I4)*, 2022, pp. 1–7. https://doi.org/10.1109/c2i456876.2022.10051317

[18] G. Mohammed Salem and C. Djilali, "Automation and remote control of a smart greenhouse," 2023. https://dspace.univ-adrar.edu.dz/jspui/handle/123456789/8735

[19] W. T. Sung, I. V. Devi, and S. J. Hsiao, "Early warning of impending flash flood based on AIoT," *EURASIP J. Wirel. Commun. Netw.*, vol. 2022, no. 1, p. 15, 2022. https://doi.org/10.1186/s13638-022-02096-5

[20] Y. Suppakhun, "Flood surveillance and alert system an advance the IoT," in *2019 IEEE Asia Pacific Conference on Circuits and Systems (APCCAS), Bangkok, Thailand*, 2019, pp. 325–328. https://doi.org/10.1109/apccas47518.2019.8953179

[21] D. Saranya, P. Chinnasamy, G. Nalinipriya, P. N. Jeipratha, D. C. J. W. Wise, and A. Kalaiarasi, "Adaptive intelligence system based on the Internet of Things for patient monitoring in remote area," in *2022 International Conference on Computer Communication and Informatics (ICCCI), Coimbatore, India*, 2022, pp. 1–6. https://doi.org/10.1109/iccci54379.2022.9741062

[22] C. Mariki, "Fetal heart beat rate monitoring support device for pregnant women diagnosed with mild pre-eclampsia/hypertension in Tanzania," 2022. https://doi.org/10.58694/20.500.12479/1581

[23] R. Jain, "Getting started with OpenCV," in *Advanced Home Automation Using Raspberry Pi: Building Custom Hardware, Voice Assistants, and Wireless Nodes*, 2021, pp. 267–296. https://doi.org/10.1007/978-1-4842-7274-9_8

[24] M. I. Tawakal, M. Abdurohman, and A. G. Putrada, "Wireless monitoring system for motorcycle tire air pressure with pressure sensor and voice warning on helmet using fuzzy logic," in *2021 International Conference on Software Engineering and Computer Systems and 4th International Conference on Computational Science and Information Management (ICSECS-ICOCSIM), Pekan, Malaysia*, 2021, pp. 47–52. https://doi.org/10.1109/icsecs52883.2021.00016

[25] S. Yang, D. Xiang, A. Bryant, P. Mawby, L. Ran, and P. Tavner, "Condition monitoring for device reliability in power electronic converters: A review," *IEEE Trans. Power Electron.*, vol. 25, no. 11, pp. 2734–2752, 2010. https://doi.org/10.1109/tpel.2010.2049377

[26] P. William Rey and D. Kieth Wilhelm Jan Rey, "AZKALS: Revolutionizing pet care with an IoT-powered smart dog cage management system," in *2024 3rd International Conference on Computer Technologies (ICCTech), Bali, Indonesia*, 2024, pp. 48–54. https://doi.org/10.1109/icctech61708.2024.00019

[27] S. Hao, W. Hao, J. Fu, F. Jiang, and Q. Zhang, "Landslide monitoring and early warning system based on edge

computing," *IOP Conf. Ser.: Earth Environ. Sci.*, vol. 861, no. 4, p. 042056, 2021. https://doi.org/10.1088/1755-1315/861/4/042056

[28] P. Juneja, "Applicability of remote sensing network (WSN) technology in the early detection of landslides," *Int. J. Profess. Studies*, vol. 2019, no. 8, pp. 34–40, 2019.

[29] E. A. Oguz, K. Robinson, I. Depina, and V. Thakur, "IoT-based strategies for risk management of rainfall-induced landslides: A review," in *Proceedings of the 7th International Symposium on Geotechnical Safety and Risk (ISGSR 2019), Taipei, Taiwan*, 2019, pp. 733–738. https://doi.org/10.3850/978-981-11-2725-0-is13-2-cd

[30] M. Ragnoli, P. Esposito, V. Stornelli, G. Barile, E. D. Santis, and N. Sciarra, "A LoRa-based Wireless Sensor Network monitoring system for urban areas subjected to landslide," in *Proceedings of the 2023 8th International Conference on Cloud Computing and Internet of Things, Okinawa, Japan*, 2023, pp. 91–97. https://doi.org/10.1145/3627345.3627359

[31] D. K. Yadav, P. Mishra, S. Jayanthu, and S. K. Das, "Fog-IoT-based slope monitoring (FIoTSM) system with LoRa communication in open-cast mine," *IEEE Trans. Instrum. Meas.*, vol. 70, pp. 1–11, 2021. https://doi.org/10.1109/tim.2021.3126018

[32] M. Prasad Pujar, M. Umesh Kulkarni, M. Raviraj Kulkarni, and H. Harish Kenchannavar, "Internet of Things-based disaster management system," *Nanotech. Smart Remo. Net. Disas. Preven.*, vol. 2022, pp. 59–84, 2022. https://doi.org/10.1016/b978-0-323-91166-5.00011-2

[33] B. Dini, G. Bennett, A. Franco, M. Whitworth, K. Cook, A. Senn, and J. Reynolds, "Development of smart boulders to monitor mass movements via the Internet of Things: A pilot study in Nepal," *Earth Surf. Dyn.*, vol. 9, no. 2, pp. 295–315, 2020. https://doi.org/10.5194/esurf-2020-78

[34] M. M. Timbul Sigiro, I. P. Manalu, G. I. Wowiling, S. M. Silalahi, E. S. Sinambela, and F. Simatupang, "Improving road safety in landslide prone areas: Real-time LoRa-based landslide detection and warning system," in *2023 29th International Conference on Telecommunications (ICT), Toba, Indonesia*, 2023, pp. 1–5. https://doi.org/10.1109/ict60153.2023.10374074

[35] R. Toapanta, J. Chafla, and A. Toapanta, "Physical variables monitoring to contribute to landslide mitigation with IoT-based systems," in *Proceedings of ICAETT 2020, Riobamba, Ecuador*, 2020, pp. 58–71. https://doi.org/10.1007/978-3-030-63665-4_5